Droplet microfluidic hydrogen/deuterium exchange for investigating protein dynamics with millisecond precision

Dietmar Hammerschmid^a, Alistair Bailey^{b,d}, Jakub Sys^a, Simon I.R. Lane^{c,d}, Max Saito^b, Theo Hornsey^a, Niall Hanrahan^{c,d}, Andy van Hateren^{b,d}, Howard Broughton^e, Alfonso Espada^e, Eamonn Reading^{a,d} and Jonathan West^{b,d}

ORCIDs

Dietmar: 0000-0002-0210-3690

Alistair: 0000-0003-0023-8679

Jakub: 0000-0003-2589-1631

Simon: 0000-0002-8155-0981

Max: 0000-0002-5609-1445

Theo: 0000-0001-9434-4506

Niall: 0000-0002-3596-7049

Andy: 0000-0002-3915-0239

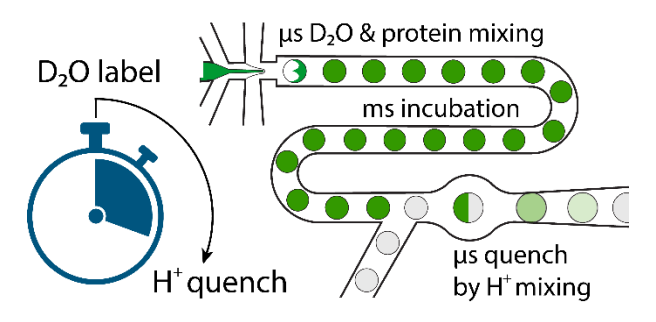
Howard: 0000-0002-3293-3775

Alfonso: 0000-0002-8301-1201

Eamonn: 0000-0001-8219-0052

Jonathan: 0000-0002-5709-6790

Graphical Abstract



^a School of Biological Sciences, Faculty of Environmental and Life Sciences, University of Southampton, SO17 1BJ, UK

^b Cancer Sciences, Faculty of Medicine, University of Southampton, SO17 1BJ, UK

^c School of Chemistry, Faculty of Engineering and Physical Sciences, University of Southampton, Southampton SO17 1BJ, UK

 $^{^{}m d}$ Institute for Life Sciences, University of Southampton, SO17 1BJ, UK

^e Centro de Investigación Lilly, SA, Avenida de la Industria 30, 28108, Alcobendas, Spain

Abstract

Hydrogen/deuterium exchange (HDX) methods for studying protein dynamics would benefit from millisecond-scale incubations to probe intrinsically disordered proteins, highly dynamic regions and conformation changes. Here we investigate droplet microfluidics for rapid mixing to trigger D_2O labelling, uniform incubations and rapid droplet merging for acid quenching in advance of mass spectrometry. A surfactant-free merging approach combining expansion elements for synchronised droplet collision proved robust. The high diffusive flux of D_2O and protons enable microsecond mixing to trigger and arrest D_2O labelling, respectively, affording the possibility of single millisecond incubations. Droplet HDX processors were used to measure the fast uptake characteristics of a model peptide. Forward exchange measurements demonstrate D_2O labelling to be the rate-limiting step, in essence defining 10 milliseconds as the minimum practical incubation time. With the ability to access millisecond time scales the fast dynamics of calmodulin, a model of calcium-triggered allostery with rapid conformational switching, was investigated. Fast reorganisation of the EF-hand motifs provoked by calcium binding was observed. The millisecond precision of droplet microfluidic HDX paves the way to advance understanding of protein structural dynamics.

Introduction

Protein motion enables function, with celebrated examples being the oar-like stroke of myosin during muscle contraction, ATP synthase rotation and the valving of ligand-gated ion channels. We have a vast library of high-resolution protein structures, largely determined using crystallography, yet we know relatively little about protein motion. This knowledge gap represents an enormous arena for discovery and opportunity to advance biotechnology, inform the development of new drugs (e.g. shifting conformational equilibria towards health), and the design of synthetic proteins. While time-resolved crystallography is maturing and delivers atomic resolution¹, routine access to beamlines with appropriate infrastructure and the pre-requisite for large quantities of well-formed protein crystals limit our ability to broadly understand protein dynamics. Instead, time-resolved cryo-electron microscopy (cryo-EM) is emerging²⁻⁶ and complements a battery of methods providing insight into protein motion. Of these, a technique called Hydrogen-Deuterium eXchange (HDX) has its place. Here labile hydrogen atoms on the amide backbone are replaced by deuterium atoms from the surrounding solvent. These can be measured by nuclear magnetic resonance (NMR) or mass spectrometry (MS) and reflect backbone malleability and accessibility from which protein structure and dynamics can be inferred. HDX-MS is gaining popularity across academic and pharmaceutical sectors owing to improved throughput, reduced sample consumption and capacity for analysing complex samples. 7,8

The HDX experiment involves (i) mixing protein with D_2O (deuterium), (ii) defined incubation periods, and then (iii) mixing with acid quenching buffer to preserve D_2O incorporated into the amide backbone for (iv) bottom-up peptide level analysis, typically by mass spectrometry. Protein structure governs the hydrogen bonding network stability and solvent accessibility which in turn dictate D_2O uptake. Exchange occurs at all time scales with the cumulative extent reflecting structural dynamics. At stably structured regions the breakage of backbone hydrogen bonds is infrequent, requiring long periods for the HDX reaction to introduce D_2O . In contrast, unstructured regions are exposed and show low level backbone stabilisation allowing the HDX reaction to introduce D_2O within short timescales. Conventional HDX workflows are limited to multi-second incubations, thereby overlooking important protein structural features. Crucially, millisecond timescales also correspond to protein folding⁹, allosteric regulation¹⁰ and intrinsic disordering¹¹. Millisecond HDX incubations also makes possible time-resolved non-equilibrium measurements involving pulsed (triggered) experiments, with the enticing possibility to observe motions arising from biomolecular interactions such as ligand binding and substrate catalysis.^{7,12,13}

To access single second and millisecond timescales manual or robotic processing in wells is replaced with continuous flow approaches within capillaries or microchannels. Examples include quenched flow-like arrangements^{9, 14, 15}, or laminar flow systems with mixing plugs housed in capillaries ¹⁶⁻¹⁸ or *in situ* fabricated porous monoliths¹⁹ within microchannels which provide narrow, convoluted paths to reduce mixing times. Recently, turbulent transport in capillaries is used for rapid mixing in an online, fully automated HDX-MS platform^{11, 20}. Within these examples, multi-fold challenges and associated drawbacks emerge: the requirement for rapid mixing (substantially faster than incubations), uniform incubation times, reliability and low sample consumption coupled with simple and low-cost instrumentation. Cost and sample consumption are key factors which preclude wider access to the HDX community. To date, the shortest achievable incubation with these methods is 50 milliseconds^{16, 20}, providing motivation to explore methods for shorter incubations which necessarily require exceptionally fast mixing.

In this study we turn our attention to droplet microfluidics, famed for rapid mixing enabled by circulations within droplets 21,22 . In addition, single-file droplet transport by channel confinement bypasses the Taylor-Aris dispersion 23,24 problem encountered with ordinary microfluidics, to achieve extremely uniform incubations 21,22,25,26 . The remaining challenge is the need to rapidly introduce and mix quench buffer with the protein/ D_2O droplets at a precisely defined time, which can be achieved by droplet merging. We have considered passive methods involving straightforward and inexpensive fabrication, reduced instrumentation and complexity to favour user uptake. In this study, we explore 3 approaches for rapidly introducing quench buffer to high-velocity D_2O /protein droplets and identify a surfactant-free droplet collision approach as being the most robust. We demonstrate microsecond mixing, facilitating incubations as short as 1 millisecond. The ability to access such short timescales with high temporal precision in an expensive format requiring minimal sample will be of interest for the community to study highly dynamic proteins, non-equilibrium measurements or dynamics underpinning catalysis. Using this improved temporal resolution we experimentally explore the limits of D_2O labelling and compare results

with theory. To test drive droplet microfluidic HDX for probing highly dynamic regions, we investigated calmodulin, a model of calcium-mediated allostery with rapid shape change.

Materials and Methods

Microfluidic Design

Devices consist of a droplet generation junction for adding D_2O to protein, then an incubation channel (with length and velocity defining time) which concludes by joining with a channel for introducing quench buffer to arrest labelling (SI Figure S1). The 'chop and exchange' device has adjoining channels downstream for the addition of perfluoro-2-octanol, which exchanges with the surfactant at the droplet interface to cause droplets in contact to merge (Figure 1A). The 'drag and merge' device simply relies on a carrier fluoro-oil without surfactant, with protein/D₂O droplets contacting a stream of quench buffer to produce daughter droplets containing near-equivalent volumes of both (Figure 1B). The 'collide and merge' device employs two droplet generation junctions, one for producing protein/D2O droplets and the other for producing quench droplets. Droplets are again produced using fluoro-oil without surfactant and merge upon collision, either where channels converge, or moments downstream in a channel expansion-contraction element where lateral oil drainage allows droplets to contact one another and merge (SI Figure S2A, Figures 1C and 2B). For short, 1 millisecond incubations, smaller and higher velocity droplets are required for mixing in the order of 100 microseconds. These small and fast droplets require steering towards the channel centre to ensure droplets contact one another for reliable mixing. This was achieved using pillar structures previously described by Niu et al^{27} (SI Figure S2B and Figure 2D) which facilitate lateral oil drainage, while positioning droplets at the channel centre.

Microfabrication and Assembly

Droplet microfluidic HDX devices were fabricated in poly(dimethylsiloxane) (PDMS, Sylgard 184) by standard soft lithography using SU-8 on silicon masters. Devices for 10- and 100-millisecond incubations were fabrciated with a height of 41 μ m, and with a channel width of 75 μ m and a droplet junction width of 40 μ m. The 'collide and merge' device has a channel expansion element with a 600 μ m. The 'collide and merge' device for 1 millisecond incubations was fabricated to a height of 14 μ m, and with a channel width of 30 μ m, a droplet junction width of 15 μ m, and with a 21- μ -volume cavity with oil-drainage pillars (SI Figure S2B). PDMS was cured on the SU-8 wafer at 60 °C for 2 hours and a counter-moulding strategy was used to produce polyurethane masters²⁸. Using these, PDMS was again cured at 60 °C for 2 hours, then tubing ports were introduced using 1-mm-diameter biopsy punches (Miltex, Williams Medical Supplies Ltd). A 1.5-mm-diameter biopsy punch was used for the exit port. Devices were bonded to glass microscope slides using a 30 s oxygen plasma treatment (Femto, Diener Electronic) followed by channel surface passivation using 1% (v/v) trichloro(1 μ 1,1 μ 2,2 μ 2-perfluorooctyle) silane (Merck) in HFE-7500 (3M Novec).

Microfluidic Operation

Syringe pumps (Fusion 100, Chemyx) were used to deliver reagents from gas tight syringes (SGE) to the droplet microfluidic HDX device. Syringes were fitted with 25 gauge (OD 0.5 mm) needles for interfacing with polytetrafluoroethylene (PTFE, Bohlender^{IM}, Merck) tubing with an ID of 0.5 mm. The 1 mm OD of the tubing allows secure attachment, by insertion, into the device ports. For retrieving sample from the device, 1.6 mm OD PTFE tubing (Cole-Palmer) was used which fits securely in the 1.5-mm-diameter exit port. This tubing has a 0.3 mm ID for rapid sample delivery to a 0.5 mL microcentrifuge tube placed in a 3D printed (UltiMaker Cura) dry ice bath designed to sit on the microscope stage in close proximity to the microfluidic HDX device. Tubing connects to a hole in the microcentrifuge tube lid prepared using a biopsy punch. Tubing should not be inserted to the bottom of the microcentrifuge tube to avoid sample freezing within the tubing and blocking flow. Once collected, volumes were flash frozen in liquid nitrogen and stored at -80°C prior to mass spectrometry. Droplet generation and merging was monitored using a high-speed camera (Phantom Miro M310, Vision Research) mounted on an inverted microscope (Olympus, CKX53). A 9:1 ratio of D_2O to protein volume was used for labelling and a 1:1 ratio of D_2O /protein to quench buffer volume was

used to quench labelling. Liquids and flow rates for the different microfluidic HDX methods are documented in Table 1.

Table 1. Microfluidic HDX methods, incubation channel dimensions and liquids. The carrier phase for droplet generation was 1% QX200 (BioRAD, providing surfactant) in HFE-7500 (3M Novec) or just HFE-7500. The surfactant in QX200 was exchanged using neat perfluoro-1-octanol (PFO, Merck). A 100 μ L aqueous volume was required for MS measurements, involving 5 minute processing times for the 10 and 100 ms incubation devices and 20 minute processing times for the 1 ms device.

Microfluidic Method	Channel height (μm)	Channel width (μm)	Fluoro-oil flow rate (µL/min)	Protein flow rate (μL/min)	D ₂ O flow rate (μL/min)	Quench flow rate (μL/min)	Other flow rates (µL/min)
Chop & Exchange	43	75	25 (1% QX200)	1	9	10	8 (PFO)
Drag & Merge	43	75	25 (HFE-7500)	1	9	10	-
Collide & Merge (10-100 ms)	41	75	20 (HFE-7500)	1	9	10	20 (HFE-7500)
Collide & Merge (1 ms)	14	30	7.5 (HFE-7500)	0.25	2.25	2.5	7.5 (HFE-7500)

Mixing Analysis

A red dye, sulfanilic acid azochromotrop (SAA, Merck, λ_{max} 505–510 nm, 10 mM), was used to understand mixing times during droplet generation and droplet merging. Fluorescein pH-switching²⁹ was used to estimate protein mixing times with D₂O during droplet generation and protein/D₂O mixing times with acid quench buffer during droplet merging: Addition of 1M hydroxide to acidified 10 mM fluorescein neutralises the solution and restores fluorescent emission (λ_{max} 517 nm), whereas addition of 10 mM HCl (pH 2.0) to 10 mM fluorescein switches off fluorescence. Here the hydroxide (M_{wt} 17 Da) closely matches the diffusivity of D₂O (M_{wt} 20 Da) and HCl addition mimics the quenching reaction. A sensitive camera (Fusion, Hamamatsu) mounted on an inverted fluorescent microscope (CKX41, Olympus) was used for fluorescent imaging with peak excitation at 490 nm (pE-100 CoolLED) and emission collection at 515±10 nm. A 200 ms exposure was used to collect fluorescent emission from large numbers of droplets in a single frame (~300 large droplets (~110 pL) and ~3,000 small droplets (~3 pL)) to provide ensembled measurments. The plot profile function in Fiji was used to quantify fluorescence development during droplet generation and fluorescence reduction following droplet merging. Position data was converted to time using channel location-determined velocities.

Millisecond Labelling of Peptides

Peptide AEAKQNLGNAKQK (Synpeptide) was solubilised in equilibration buffer (20 mM HEPES, pH 7.4) at a concentration of 1 μ M. D₂O labelling was performed for 10 and 100 millisecond as described in the microfluidic operation section using a 9:1 ratio of labelling buffer (20 mM HEPES in D₂O, pD 7.4) to peptide volume and a 1:1 ratio of D₂O/protein to quench buffer (100 mM NaH₂PO₄, pH 2.3) volume. Samples were collected for 5 minutes on dry ice, flash frozen in liquid N₂ and stored at -80 °C in readiness for mass spectrometry. A control sample was prepared by 10-fold dilution in equilibration buffer before mixing 1:1 with quench buffer.

Forward Exchange Measurements

Back exchange, the loss of deuterium label from the amide backbone, and gain of deuterium label after quench, so-called forward exchange, can occur with delays between quench and analysis. Although slow forward exchange becomes problematic when the amount of deuterium label incorporated into the protein is low, a consequence of short labelling times. To measure forward exchange we added D_2O at the quench step³⁰, not the initial step. Uptake was quantified at peptide level after calmodulin pre-digestion: Bovine calmodulin (CaM, recombinant, expressed in *E.coli*, Cat No. C4874-1MG, Merck) was solubilized at 1 mg/mL in equilibration buffer (20 mM HEPES, pH 7.4) and mixed 1:1 with quench buffer (100 mM NaH₂PO₄,

pH 2.3) to a final concentration of 2 and 20 µM for forward exchange and standard labelling, respectively. Quenched CaM digestion was performed on an ACQUITY UPLC System with HDX Technology (Waters, Wilmslow, UK). The HDX manager of the system was equipped with a self-packed guard column (2.0 mm ID x 2 cm unpacked; Part No. C-130B) containing immobilized pepsin agarose resin (Cat No. 20343, Thermo Fisher). Samples were injected into the HDX manager and run with solvent A (0.23% formic acid, pH 2.5) over the self-packed pepsin column at 200 µL/min. Digested CaM was collected for 1 minute at the column outlet, flash frozen in liquid N2 and freeze-dried for 16 hours overnight. For mass spectrometry, samples were resuspended in 100 μL equilibration buffer and sonicated for 15 minutes. Standard and forward exchange labelling were then performed on the respective droplet microfluidic HDX device (1, 10, and 100 millisecond). Standard labelling was performed as described in the microfluidic operation section using a 9:1 ratio of labelling buffer (20 mM HEPES in D₂O, pD 7.4) to protein volume and a 1:1 ratio of D₂O/protein to quench buffer (100 mM NaH₂PO₄, pH 2.3) volume. For forward exchange labelling, quench buffer was prepared in 90% D₂O (100 mM NaH₂PO₄, pD 2.3) to reach an equal deuterium content in the final sample. Labelling experiments were repeated at pD 9.4 using 20 mM sodium carbonate-bicarbonate D₂O labelling buffer (pD 9.4) and 1.25% formic acid quench buffer. The flow rates for the 10 and 100 millisecond incubations require 5 minutes to collect 100 μ L aqueous volume, whereas the lower flow rate for the 1 millisecond incubation required 20 minutes to collect this volume. Using different tubing lengths, transport time from device exit to collection on dry ice was standardised to 20 seconds. Once collected samples were flash frozen in liquid N2 and stored at -80 °C in readiness for mass spectrometry.

Investigating Calmodulin Dynamics

Calmodulin (CaM) was solubilised at 1 mg/mL in equilibration buffer (20 mM HEPES, pH 7.4). To remove any trace Ca²⁺, 1 mM ethylenediaminetetraacetic acid (EDTA) was added to the sample and incubated for 16 hours at room temperature. CaM was purified by gel filtration using a Superdex 200 Increase 10/300 GL column (Cytiva, Amersham, UK). Fractions containing CaM were pooled and stored at -80 °C until use (gel filtration resulted in a 4-fold dilution). CaM dynamics was investigated with and without Ca2+, and nonequilibrium (Ca²⁺ was introduced during D₂O labelling) protein states at millisecond to second time scales (10 and 100 millisecond microfluidic, 1 second manually, and 10 seconds robot labelling). Ca²⁺-bound CaM was prepared by adding 1 mM CaCl₂ and incubation at room temperature (22 °C) for at least 3 hours prior to deuterium labelling. CaM without Ca²⁺ and all buffers were also equilibrated to room temperature. After equilibration, the exchange reaction was initiated by 10-fold dilution into deuterated labelling buffer (20 mM HEPES, pH_{read} 7.0), yielding a 90% deuterium content in the final reaction mixture. Ca²⁺-bound CaM and non-equilibrium protein states were deuterated with Ca²⁺-labelling buffer (20 mM HEPES, 1 mM CaCl₂, pH_{read} 7.0). Reactions were quenched by 1:1 dilution with quench buffer (100 mM NaH₂PO₄, pH 2.3). Samples incubated for millisecond time scales (10 and 100 milliseconds) were processed as described above (microfluidic operation), with the exception of 8 second transport times from device to dry ice. Samples for 1 second manual labelling were performed by subsequent addition of labelling and then quench buffer within 1 second, followed by direct flash-freezing in liquid N2. 10 second labelling was performed by the LEAP PAL robot with HDX automation (Trajan, Milton Keynes, UK). All protein states and labelling time points were performed in three technical replicates on two occasions. Samples processed by microfluidic and manual methods were stored at -80 °C for a maximum of 24 hours prior to mass spectrometry.

Mass Spectrometry Measurements

Measurements were performed on an ACQUITY UPLC M-Class System with HDX Technology (Waters, Wilmslow, UK) directly coupled to a Xevo G2-XS QToF Mass Spectrometer (Waters, Wilmslow, UK). Frozen samples were quickly thawed, and the aqueous phase (top layer) was injected into the HDX manager. Samples obtained after automated D_2O labelling were injected by the LEAP PAL robot directly after quench. Proteins were digested on-line using a self-packed pepsin (immobilized pepsin agarose resin, Cat No. 20343, Thermo Fisher) column (2.0 mm ID x 2 cm unpacked; Part No. C-130B) at 15 °C, and resulting peptides were trapped/washed on an Acquity UPLC BEH C18 VanGuard pre-column (1.7 μ m, 2.1 mm x 5 mm, Waters, Wilmslow, UK) for 3 min at 200 μ L/min. The self-packed pepsin column was replaced by a

union for samples containing pre-digested calmodulin (*i.e.* all samples for comparing forward exchange with standard labelling). Peptides were eluted and separated on an Acquity UPLC BEH C18 analytical column (1.7 μ m, 1.0 mm x 100 mm, Waters, Wilmslow, UK) with a linear gradient over 7.5 minutes from 8 to 35% solvent B (0.23% formic acid in acetonitrile) at a flow rate of 40 μ L/min and at 0 °C. To prevent peptide carryover, the pepsin column was washed twice during the linear gradient using a pepsin wash solution (1.6 M guanidine-HCl, 4% acetonitrile, and 0.8% formic acid, pH 2.5). Further, chromatographic columns were washed after each sample run by applying a saw-tooth gradient.

HDX-MS Data Analysis

For peptide identification, undeuterated calmodulin was injected into the system applying the same settings for protein digestion and chromatographic separation. Peptides were measured in positive ion mode and MS^E analysis was applied with a ramped collision energy from 20 to 45 V. Sodium iodide and leucine enkephalin were used for calibration and mass accuracy correction, respectively. Raw data from MS^E runs were analyzed with ProteinLynx Global Server (PLGS) 3.0 (Waters, Wilmslow, UK). Identified peptides were loaded into DynamX 3.0 (Waters, Wilmslow, UK) and filtered as follows: minimum intensity: 1481, sequence length: 5–25, minimum products per amino acid: 0.11, minimum consecutive products: 1, minimum score: 6.62, maximum MH+ error: 10 ppm, file threshold: 4 out of 5 measurements³¹. Peptides were manually curated to exclude MS traces of poor quality or false identifications. Subsequently, raw data from deuterated samples (with and without Ca²⁺ and non-equilibrium) were loaded to calculate the deuterium uptake at peptide level. To determine statistically significant differences in deuterium uptake between two protein states, a global 99% confidence threshold was calculated based on a previous approach³² including recently proposed corrections³³. The mass spectrometry proteomics data have been deposited to the ProteomeXchange Consortium via the PRIDE³⁴ partner repository with the dataset identifier PXD063880.

Results and Discussion

Droplet Merging Strategies

Achieving millisecond HDX incubations requires rapid mixing of protein with D_2O , defined incubations and subsequently rapid mixing with acid quench buffer. While droplet microfluidics enable rapid mixing and precisely defined incubations, the task of reliable droplet merging at the correct position (*i.e.* time) and at high velocity for rapid mixing required investigation. Several on the fly droplet merging methods have been developed. Surface free energy patterning within microchannels presents a hydrophilic stripe for droplet trapping and merging^{35, 36}. Alternatively, electrocoalescence reliably achieves merging at a defined location³⁷⁻⁴¹. In pursuit of straightforward, low-cost fabrication and instrumentation to favour end-user adoption we instead chose to investigate passive methods. Initial experiments used depleted surfactant to allow the aqueous compartments of two droplets to contact one another and coalesce^{42, 43}. However, reliability issues emerged and the merging position varied, introducing variable incubations. We next investigated other passive droplet merging techniques and their suitability for fast HDX.

We first explored the injection of quench buffer from a side channel into passing droplets that were generated upstream 44,45 . Using low concentration surfactant (1% QX200 in HFE-7500), droplet momentum and interfacial tension acts like a chopper, producing a second droplet of quench buffer which is synchronised with the D_2O droplet. Merging at a defined downstream location is achieved by the introduction of perfluoro-1-octanol (PFO), a weak surfactant which exchanges with the QX200 surfactant, momentarily producing surfactant-free pin holes at the interface between droplets to trigger merging ('chop and exchange' method, Figure 1A, SI video 1). However, the process was not reliable, proving to be sensitive to subtle physical and chemical variations in reagents²⁷ which either prevented chopping or merging. We next considered a more straightforward approach involving the generation of surfactant-free D_2O droplets with the injection of quench buffer into passing droplets. Here, the viscous interaction between D_2O droplets and quench buffer caused equal volumes of quench buffer to be dragged from the input stream and, in the absence of surfactant, instantly merged with the protein/ D_2O droplet ('drag and

merge' method, Figure 1B, SI video 2). Again this synchronises protein/ D_2O and quench buffer inputs, with merging at a defined position. Still, the method was vulnerable to streaming jets of quench buffer, losing positional control and the small volume circulations necessary for rapid mixing.

With the emphasis on reliability and speed we next opted to independently generate surfactant-free protein/ D_2O and quench buffer droplets at matched frequencies for pairing²⁵. However, droplets are not synchronised, either merging as channels converge or missing one another to form an alternating train of droplets. To address this, we installed a fail-safe in the form of a channel expansion-contraction element⁴⁶⁻⁴⁸. On entering the expanding channel region the droplets decelerate, and remain at the channel centre with the fluoro-oil 'draining' outwards to cause droplets to contact one another and merge in microseconds ('collide and merge' method, Figure 1C, SI video 3). The channel subsequently contracts, allowing merged droplet pairs to accelerate for faster mixing. Merging occurs in the expanding half of the cavity, with the simple design rule of the half-cavity volume (600 pL) being \geq 4 and \leq 6 droplet volumes (for a 2:1 fluoro-oil:aqueous flow ratio). This surfactant-free collide and merge strategy proved highly reliable, ensuring that all protein/ D_2O droplets merge with quench buffer either as channels converge or immediately downstream in the expansion-contraction element. Settling on this strategy, we designed HDX microfluidic circuits for 10 and 100 millsecond incubations.

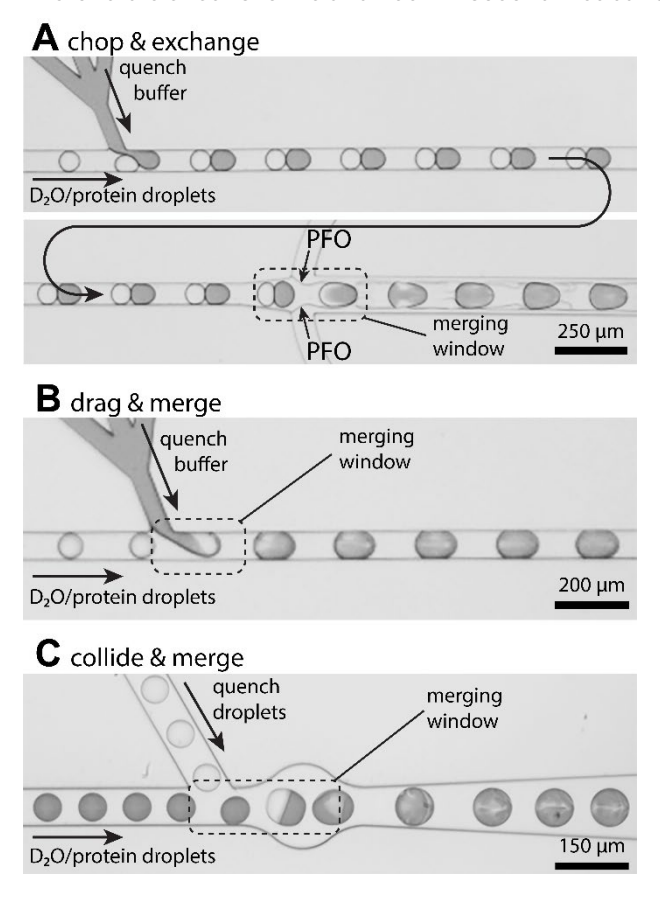


Figure 1. Droplet merging strategies. (A) 'Chop and exchange': The momentum of the first, protein/ D_2O , droplet chops off a droplet from the adjoining quench buffer channel. Perfluoro1-octanol (PFO) is introduced downstream, destabilising droplet interfaces to cause merging. (B) 'Drag and merge': Without surfactants, viscous drag between the protein/ D_2O droplet and quench buffer produces a daughter droplet with equal volumes of protein/ D_2O and quench buffer. (C) 'Collide and merge': Protein/ D_2O and quench buffer droplets are generated independently without surfactant, and merge upon collision. Channel expansion ensures all droplets merge.

For shorter, 1 millisecond incubations, faster mixing is required and was achieved by channel miniaturisation to produce smaller droplets (3 pL, see Table 1). Such small droplets provide shorter diffusion paths and also involve higher velocity transport (~795 mm/s vs ~325 mm/s for ~110 pL droplets) which enhances convection. At these scales a higher 3:1 fluoro-oil:aqueous flow ratio was required for reliable droplet generation, with the expansion cavity volume being ≥5 and ≤8 droplet volumes. In addition,

the expansion-contraction element required the inclusion of drainage pillars according to the design of Niu $et \, al^{27}$, which act to confine droplets to the channel centre to ensure merging.

Microsecond Mixing

A red dye was used to gain a first understanding of mixing for triggering D_2O labelling and mixing following droplet merging for acid quenching (Figures 1 and 2). Observations indicate millisecond scale mixing times²⁸. However, the colourimetric dye approach neglects the high diffusivity (1.7 x 10^{-5} cm²/s⁴⁹) and flux⁵⁰ of D_2O (55.5 Molar) for triggering labelling and the extremely high diffusivity of protons (9.3 x 10^{-5} cm²/s^{51,52}) during quenching. To approximate these characteristics, we used fluorescein emission (λ_{max} 517 nm) modulation by pH-switching²⁹. At pH 3 or below relative fluorescence is near zero, but as the pH increases so does the fluorescence. To mimic D_2O mixing, we combined a stream of 1 M hydroxide (M_{wt} 17 Da versus D_2O M_{wt} 20 Da) with acidified 10 mM fluorescein (pH 3) during droplet generation and imaged fluorescence development along the channel. To mimic acid quenching during droplet merging and mixing, a 10 mM HCl solution (pH 2) was combined with 10 mM fluorescein at pH 7.0. Fluorescence reduction along the channel was used to measure mixing and reaction times to mimic the overall quench process.

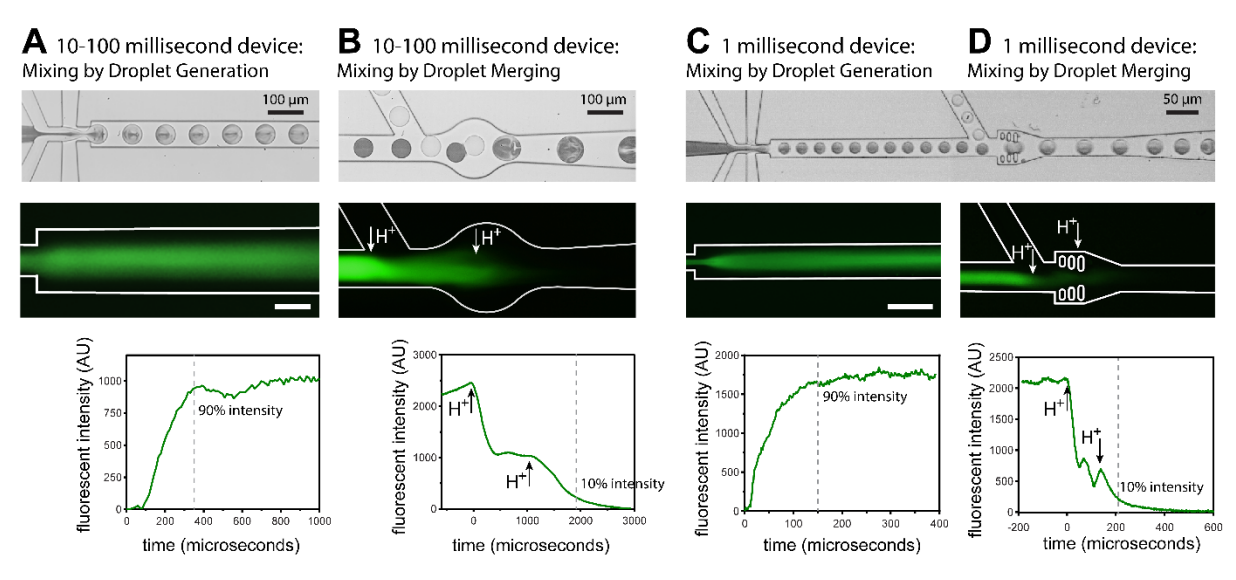


Figure 2. Mixing time analysis. (A) Droplet generation in the 10 and 100 millisecond incubation devices. Acidified fluorescein on-switching with hydroxide was used to estimate a mixing time of ~350 microseconds. (B) Droplets collide as channels converge or collide in the channel expansion region to produce two mixing times estimated using fluorescein off-switching with HCl to be ~350 microseconds and ~1 millisecond, respectively. (C) Fast mixing occurs in the 1 millisecond droplet generation device, with a fluorescein on-switching time of ~150 microseconds. (D) Droplets collide at various positions; as channels converge and in the oil drainage element. The overall fluorescein off-switching time is ~200 microseconds, with individual droplet pair mixing times being considerably less. Attaining 90% fluorescent intensity was used to estimate the D_2 0 mixing time, and reduction to 10% was used to estimate the acid mixing time. Fluorescent image scale bars represent travel durations of 25 microseconds (A) and 100 microseconds (B).

When 1 M hydroxide is used to approximate D_2O diffusion and the high flux, mixing times during droplet generation and transport are markedly reduced compared to observations with red dye. In the 10 and 100 millisecond incubation devices, mixing times are ~350 microseconds (Figure 2A). Two positions emerge for droplet merging, first where channels converge and secondly in the expanded channel region (SI Figure S2A). Using fluorescein off-switching with HCl, the first merging event has a mixing time of ~350 microseconds, with the second being extended to ~1 millisecond resulting from reduced velocity in the expansion-contraction element (Figure 2B). These mixing times are suitably fast to plausibly define 10 and 100 millisecond incubations (i.e. substantially shorter than the incubation times).

Shorter incubations required faster mixing achieved by droplet miniaturization. Mixing during droplet generation in the 1 millisecond incubation device was decreased to ~150 microseconds (Figure

2C). Merging occurred at channel convergence and the oil-drainage pillars, overall producing a mixing time of 200 microseconds (Figure 2D). With ensembled measurements involving ~3,000 droplets for each location, the mixing times of individual droplet pairs cannot be imaged. However, the sharp drop in fluorescence when channels first converge indicates <50 microseconds mixing times and ~100 microseconds when transported within the lower velocity pillar structure (Figure 2D, SI Figure S2B). Again, these are suitably fast for single millisecond incubations. Incubations shorter than 1 millisecond could be accessed using smaller and still faster droplets but will be hampered by difficulties of synchronizing smaller droplet pairs at a given location and for sufficient time for oil drainage to allow droplets to contact and merge. Indeed, 1 millisecond incubations may likely prove the limit for reliable droplet processing.

Millisecond Calibration with Peptides

With precision millisecond incubations afforded by droplet microfluidic HDX, we went on to test millisecond D_2O labelling of peptides. Ordinarily peptides do not have secondary structure, providing random-coil characteristics that allows for comparison of the measured D_2O uptake with theoretical exchange. Using droplet microfluidics, we labelled a peptide (AEAKQNLGNAKQK) for 10 and 100 milliseconds. D_2O uptake is evident (+2.26 Da) with an incubation of 10 milliseconds and increases (+5.44 Da) with an incubation of 100 milliseconds (Figure 3A). This demonstrates the value of droplet microfluidic HDX for capturing time-dependent differences in uptake of highly dynamic peptides and protein regions. Measurements are higher than theory predicts, although in agreement with those produced using a high-velocity quenched flow apparatus (Figure 3B)²⁰.

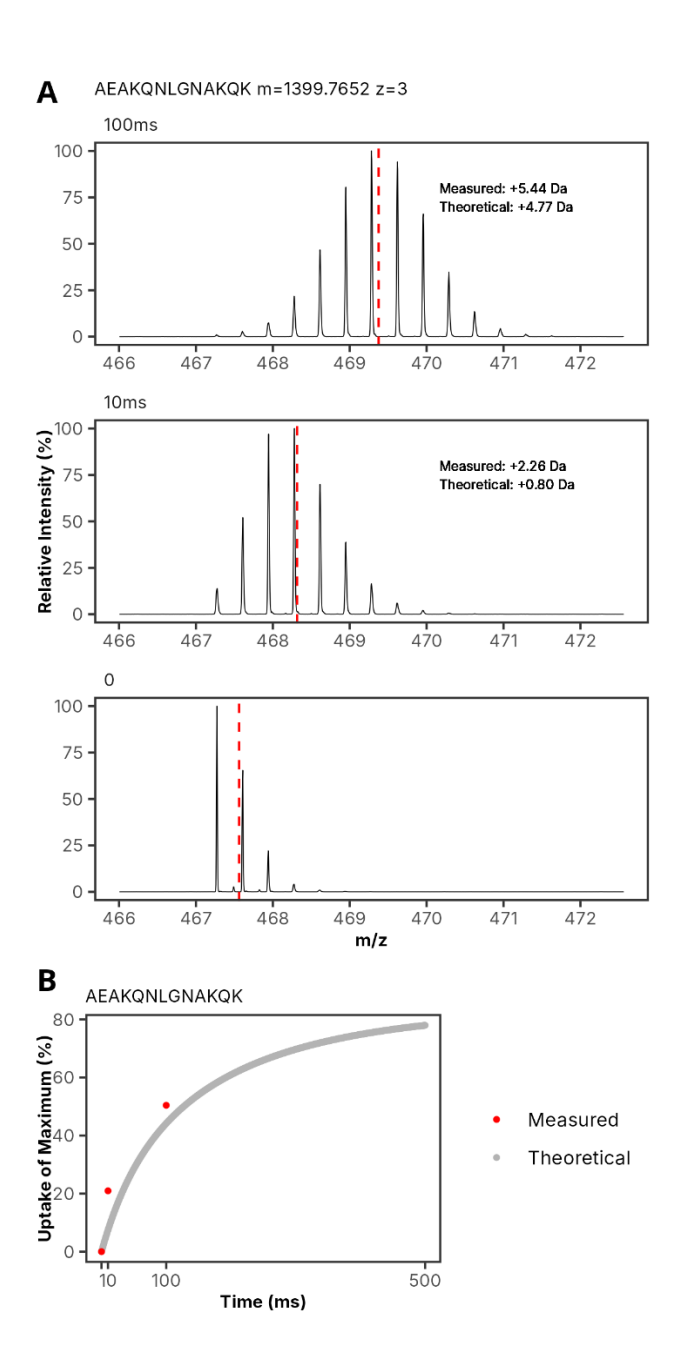


Figure 3. Millisecond HDX of Peptides. (**A**) Stacked spectral plot of charge state +3 of peptide (AEAKQNLGNAKQK, [M+H]⁺ 1399.7652) at 0, 10, and 100 millisecond incubations from bottom to top. The red dashed line indicates the centroid and measured as well as theoretical uptake values are displayed. (**B**) Theoretical chemical exchange of peptide (AEAKQNLGNAKQK) at pD 7.4 and 22 °C from 0 to 500 millisecond. The red dots indicate the measured values at 10 and 100 milliseconds.

Incubation Limit

We went on to determine the minimum possible incubation time point using calmodulin peptides. Upon acid quenching, D_2O exchange rates are reduced by 5–6 order of magnitude but can nevertheless still proceed. This, so-called, forward exchange contribution can be negligible to the overall measured HDX with incubations of seconds to hours, but forward exchange becomes apparent at millisecond timescales where reduced incubations result in extremely low D_2O uptake (SI Table S1). After D_2O droplets merge with quench droplets they are transported from the device to dry ice in 20 seconds, a time sufficient for forward exchange to occur. It is therefore necessary to compare standard labelling with forward exchange to ensure that D_2O uptake during 1, 10 and 100 millisecond HDX incubations does indeed originate from labelling and not just forward exchange post-quench. For standard labelling, we used the conventional sequence of

 D_2O addition, incubation, and quench. In contrast, adding D_2O at the quench step, not the initial step, allows forward exchange to be quantified³⁰. To aid comparison between forward exchange and standard labelling experiments we worked with pre-digested CaM to provide putatively random-coil peptides.

Deuterium labelling is compared with forward exchange levels across the millisecond incubations (Figure 4A). With the 100 millisecond incubation all peptides exhibit a higher degree of D_2O labelling compared to forward exchange, demonstrating genuine labelling during incubation. However, shortening the incubations to 10 and 1 millisecond shifts the labelling to forward exchange ratio. At 10 milliseconds most peptides show a small degree of labelling relative to forward exchange (Figure 4B), whereas at the 1 millisecond time-point labelling and forward exchange levels are equally low. This is also indicated by the low theoretical labelling levels calculated for a random coil incubated with D_2O for 1 millisecond (SI Table S1). Single millisecond incubations are therefore unrealistic at physiological pH. Since exchange kinetics increase with pH, we increased the pD (pH_{read} + 0.4) from 7.4 to 9.4 while retaining the quench condition at pH 2.5. As anticipated, higher D_2O labelling was observed across the time course (Figure 4C,D). The low millisecond incubations may prove attractive for studying proteins with an alkaline optimal pH where labelling becomes saturated even at conventional second timescales^{53, 54}. To illustrate, theoretical D_2O uptake is ~100-fold higher for a 1 millisecond incubation at pD 9.4 than at pD 7.4 (SI Table S1). Taken together, we demonstrate that the lowest physiological HDX incubation is 10 milliseconds.

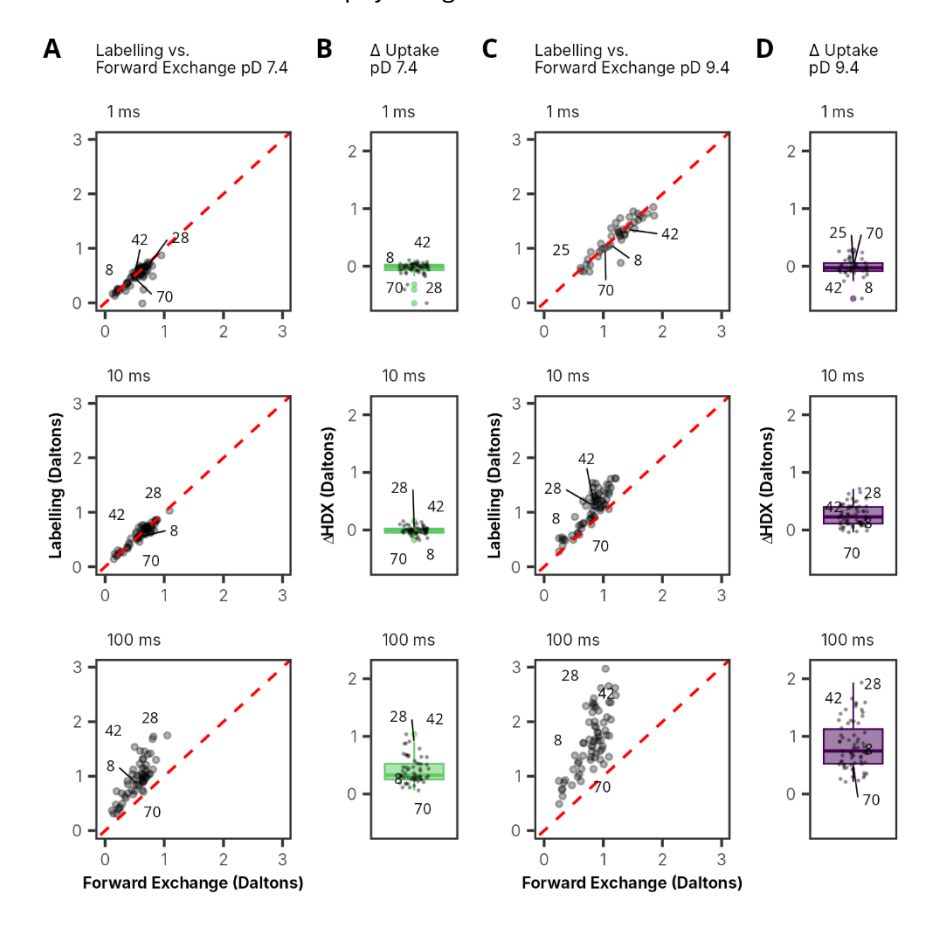


Figure 4: Time and pD-dependent labelling relative to forward exchange. (**A**) and (**C**) Parity plots of D_2O labelling versus forward exchange at 1 ms, 10 ms and 100 ms under pD 7.4 and pD 9.4 conditions. The red dashed line indicates parity of HDX between conditions and each point represents peptides identified in both conditions. Identifiers are shown for selected peptides. (**B**) and (**D**) Differential HDX of labelling versus forward exchange of each CaM peptide at 1 ms, 10 ms and 100 ms under pD 7.4 and pD 9.4 conditions.

Millisecond Incubations Capture EF-Hand Structural Reorganisations

Next, we sought to investigate CaM protein dynamics before and after the addition of Ca²⁺. CaM is a small, 148 amino acid, globular protein that has been extensively studied using various biophysical techniques⁵⁵⁻

⁵⁹. Calmodulin has two globular domains, the N- and C-lobes which are connected via a flexible linker to form a dumbbell structure^{60, 61}. Both lobes each contain two EF-hand motif Ca²⁺ binding sites⁶², and upon Ca2+ binding the linker domain becomes more flexible, enabling the N- and C- globular domains to come together in a scissor-like action⁶³⁻⁶⁵. The well-known structure and calcium-modulated conformation switching make it a model for protein dynamics and a good test case for the droplet microfluidic HDX system. We focused on short millisecond to second time points using droplet microfluidic, manual, and robot labelling. Fast labelling was performed with the 10 and 100 millisecond droplet incubations. We used the LEAP PAL-HDX robot system for 10 second D₂O incubations, the shortest possible with this instrument. Additionally, we also undertook a rapid manual mixing approach for D₂O incubations of ~1 second, sequentially adding D₂O then quench by pipette. Although the temporal accuracy of this approach is limited, we include this time point to bridge the millisecond incubations with the 10 second incubation achieved with the robot. In addition to CaM +/- Ca2+ experiments, we undertook a non-equilibrium experiment in which Ca2+ is added during D2O labelling. While ligand binding kinetics proceed at nanosecond to millisecond timescales, conformation response proceed at millisecond timescales, indicating that millisecond incubations may allow dynamic events following Ca²⁺ addition to be followed. However, comparing calmodulin samples with Ca²⁺, both loaded and non-equilibrium, did not show major differences in dynamics across the entire structure (SI Figure S3). Minimal D₂O uptake differences between loaded and non-equilibrium samples indicate fast (<10 ms) Ca2+ binding and associated structural rearrangements, consistent with observed microsecond Ca²⁺ binding kinetics⁶⁶.

Of note, peptides from the more structured EF-hand motifs show a decrease in D₂O uptake at 1 second compared to millisecond time-points (SI Figure S4), which is counter-intuitive. This stems from the different mixing methods and different time-dependent D₂O uptake characteristics. Mixing using droplet microfluidics (10 and 100 milliseconds) involves rapid convection within picolitre volumes making it fast and highly controlled for all molecules. In contrast, manual mixing for the single second incubation involves microlitre volumes with slow convection, resulting in many molecules having delayed or even no contact with D₂O before exposure to quench buffer. Critically, mass spectrometry provides an ensembled read-out of the labelled population, such that proteins unable to encounter D₂O due to poor mixing will reduce the labelling signal. It is important to consider that different structural motifs will have different timedependent uptake characteristics, with some having minimal differences in uptake across millisecond to second timescales (flat response), and others having tremendous differences (steep response). Highly flexible and accessible regions, such as the linker, remain unaffected by the poor mixing, producing, as expected, increasing uptake levels with incubations over time. Here, levels of uptake are substantially higher with one second incubations compared to millisecond incubations, such that signal losses, arising from reduced exposure times introduced by slow, manual mixing, are not immediately evident within the large, 10-fold incubation time steps. However, in structured regions with low accessibility, as in the case of the EF-hand motifs, D₂O uptake is low for both millisecond and single second incubations. Consequently, losses arising from slow, manual mixing appreciably lower the one second uptake signal. With millisecond droplet incubations, all molecules experience near instantaneous mixing, avoiding losses to produce signals which exceed the one second signal. These findings indicate the benefits of fast and complete mixing in droplets to ensure single and several second incubations, as well as the documented millisecond incubations, are indeed genuine.

We then compared CaM dynamics with and without Ca^{2^+} . The four Ca^{2^+} -binding EF-hand motif structures in the N- and C-lobes exhibit near-identical D_2O uptake responses (Figure 5A). The coordination of Ca^{2^+} is expected to provide stabilisation of the binding site, causing the formation of a less dynamic structure. This effect becomes evident with 10 second incubations and aligns with other HDX-MS studies of Ca^{2^+} -binding EF-hand motifs⁶⁷, yet the 10 millisecond labelling indicates the opposite. The millisecond time points indicate a higher uptake for Ca^{2^+} -bound CaM, which is at odds with a less dynamic conformation. This is of particular interest, as the millisecond time scale is beyond the reach of conventional labelling. The higher degree of exchange for Ca^{2^+} -bound CaM may indicate the adoption of a new conformation which enables more deuterium incorporation. Calcium binding widens the angle between helices in the EF-hand motif, forming a cleft that helps to expose the hydrophobic interface of each lobe to binding partners ^{68, 69}. Therefore, the differences observed at the 10 milliseconds time point

may shed light on the change in solvent exposure of the binding interface upon binding of Ca^{2+} . These changes in D_2O uptake are not significant for all EF-hand motifs, yet they follow the same trend and are most pronounced in the C-lobe which is known to have a higher affinity for Ca^{2+} 66, 70, 71. The calmodulin example demonstrates that short, millisecond labelling can provide valuable insights into conformational changes of proteins with fast ligand binding kinetics⁷². Other observations from the HDX-MS data stem from the longest 10 second time incubation and show increased HDX of the linker region (amino acid region 73–84) and decreased HDX of the EF2-hand of the N-terminal lobe (amino acid region 56–66) upon Ca^{2+} binding (Figure 5B). Increased HDX in the linker region reflect enhanced plasticity known to allow allostery^{73, 74}, positioning the N- and C- lobes close to one another to sample higher conformational space which allows CaM to capture a variety of different proteins⁷⁵. Reduced HDX in the EF2-hand reflects a more structured, less dynamic helix upon Ca^{2+} binding, an important feature for N-domain target binding⁷⁶.

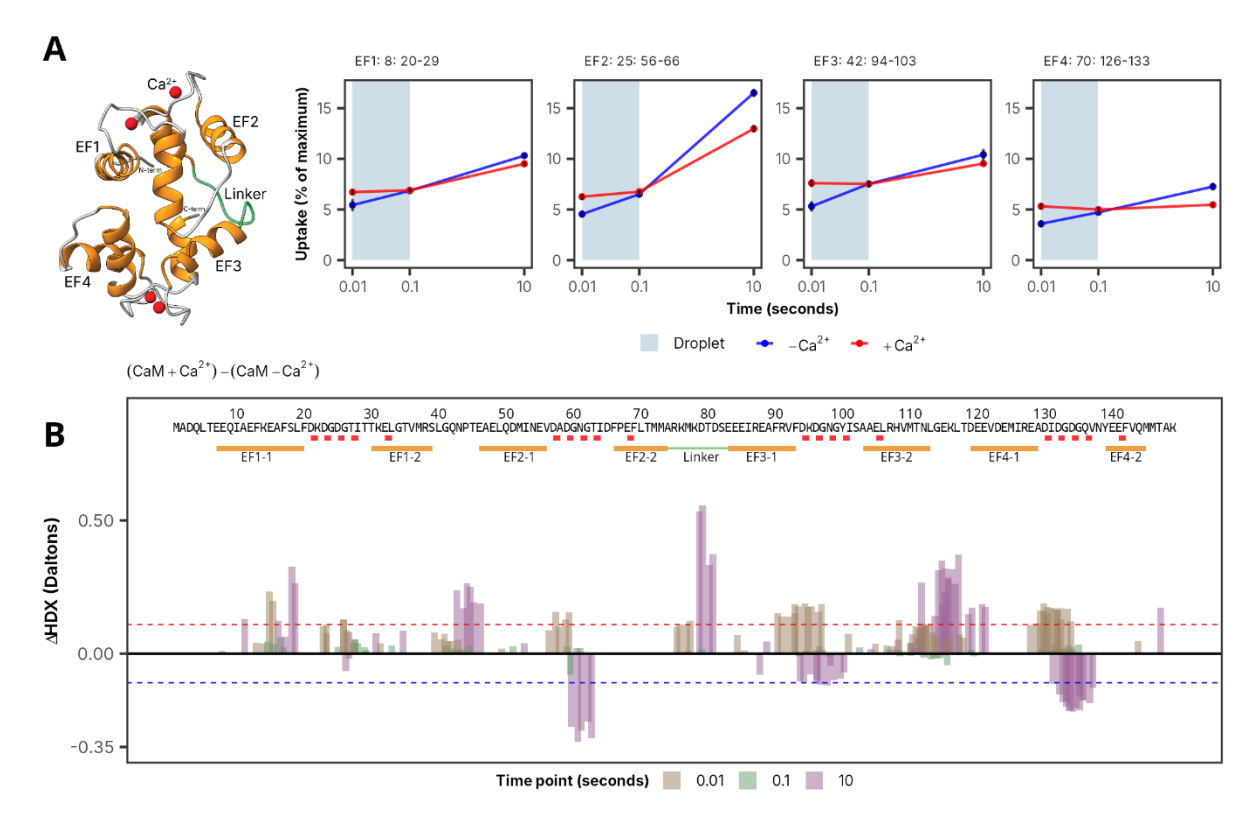


Figure 5: Calmodulin dynamics. (A) Structure of bovine CaM (PDB ID:1A29). Ca^{2+} in red, Ca^{2+} binding EF-hands in orange and Linker region in green. Inset, time-dependent D_2O labelling with Ca^{2+} (red) and without Ca^{2+} (blue) for peptides 8, 25, 42 and 70 for EF1, EF2, EF3 and EF4 regions respectively. HDX is shown as percentage of peptides' maximum theoretical uptake at 90% D_2O labelling, with the tight error bars derived from triplicate measurements. 10 and 100 millisecond incubations were processed using droplets (blue) and the 10 second incubation was processed by the robot (B) Differential HDX +/- Ca^{2+} for 80 CaM peptides at pD 7.4. Dashed lines indicate the threshold of significance for increased (red) or reduced (blue) HDX. Ca^{2+} binding sites (red), EF-hands (orange) and the Linker (green) are indicated below the CaM sequence.

Conclusions

We present a droplet microfluidics HDX approach for rapidly mixing proteins with D₂O, uniform incubations in the millisecond regime and droplet merging for rapid acid quenching. Robust droplet merging was achieved by using surfactant-free oil in combination with expansion channel elements for droplet synchronisation. The high diffusive flux of D₂O and protons allows microsecond mixing making incubations as short as 1 millisecond feasible. We show that forward exchange becomes apparent at millisecond timescales and that D₂O labelling is the rate-limiting step, indicating that 10 milliseconds is the shortest plausible physiological labelling time. Droplet HDX combined with conventional HDX was used to investigate calmodulin dynamics, with millisecond scale data indicating fast reorganisation of the EF-hand motifs triggered by calcium binding. These decoupled droplet microfluidic HDX demonstrations provide proof of principle for other lines of research investigating the dynamics of intrinsically disordered proteins, highly dynamic protein regions and conformation switching. Droplet microfluidic HDX is inexpensive and requires minimal sample, critical features enabling broad user adoption. The technology can be further advanced by integration with electrospray ionisation for direct coupling with MS to aid automation and reduce both forward and back exchange occurring outside the intended labelling window. Beyond this, we can envisage developments in both microfluidics and HDX-MS allowing protein dynamics captured within single droplets or even within single cells (i.e. a cellular 'plasticome') to be investigated.

Acknowledgements

The authors thank UKRI, BBSRC and Eli Lilly for funding. DH and ER were supported by a UKRI Future Leaders Fellowship to ER (MR/S015426/1 and MR/X009580/1). JS, ER and JW and this work were supported by Eli Lilly and Company through the Lilly Research Program, and AB, ER and JW were supported by a BBSRC grant (BB/Z51505X/1). The authors thank J.J. Philipps, Jack Stubbs and Phil Williamson for critical feedback.

References

- (1) Orville, A. M. Recent results in time resolved serial femtosecond crystallography at XFELs. *Curr Opin Struct Biol* **2020**, 65, 193-208. DOI: 10.1016/j.sbi.2020.08.011 From NLM.
- (2) Klebl, D. P.; McMillan, S. N.; Risi, C.; Forgacs, E.; Virok, B.; Atherton, J. L.; Harris, S. A.; Stofella, M.; Winkelmann, D. A.; Sobott, F.; et al. Swinging lever mechanism of myosin directly shown by time-resolved cryo-EM. *Nature* **2025**. DOI: 10.1038/s41586-025-08876-5.
- (3) Maeots, M.-E.; Enchev, R. I. Structural dynamics: review of time-resolved cryo-EM. *Acta Crystallographica Section D* **2022**, *78* (8), 927-935. DOI: doi:10.1107/S2059798322006155.
- (4) Torino, S.; Dhurandhar, M.; Stroobants, A.; Claessens, R.; Efremov, R. G. Time-resolved cryo-EM using a combination of droplet microfluidics with on-demand jetting. *Nature Methods* **2023**, 20 (9), 1400-1408. DOI: 10.1038/s41592-023-01967-z.
- (5) Klebl, D. P.; Kay, R. W.; Sobott, F.; Kapur, N.; Muench, S. P. Towards sub-millisecond cryo-EM grid preparation. *Faraday Discussions* **2022**, *240* (0), 33-43, 10.1039/D2FD00079B. DOI: 10.1039/D2FD00079B.
- (6) Banari, A.; Samanta, A. K.; Munke, A.; Laugks, T.; Bajt, S.; Grünewald, K.; Marlovits, T. C.; Küpper, J.; Maia, F. R. N. C.; Chapman, H. N.; et al. Advancing time-resolved structural biology: latest strategies in cryo-EM and X-ray crystallography. *Nature Methods* **2025**. DOI: 10.1038/s41592-025-02659-6.
- (7) James, E. I.; Murphree, T. A.; Vorauer, C.; Engen, J. R.; Guttman, M. Advances in Hydrogen/Deuterium Exchange Mass Spectrometry and the Pursuit of Challenging Biological Systems. *Chemical Reviews* **2022**, *122* (8), 7562-7623. DOI: 10.1021/acs.chemrev.1c00279.
- (8) Masson, G. R.; Burke, J. E.; Ahn, N. G.; Anand, G. S.; Borchers, C.; Brier, S.; Bou-Assaf, G. M.; Engen, J. R.; Englander, S. W.; Faber, J.; et al. Recommendations for performing, interpreting and reporting hydrogen deuterium exchange mass spectrometry (HDX-MS) experiments. *Nature Methods* **2019**, *16* (7), 595-602. DOI: 10.1038/s41592-019-0459-y.
- (9) Walters, B. T.; Mayne, L.; Hinshaw, J. R.; Sosnick, T. R.; Englander, S. W. Folding of a large protein at high structural resolution. *Proceedings of the National Academy of Sciences* **2013**, *110* (47), 18898-18903. DOI: doi:10.1073/pnas.1319482110.
- (10) Rob, T.; Gill, P. K.; Golemi-Kotra, D.; Wilson, D. J. An electrospray ms-coupled microfluidic device for sub-second hydrogen/deuterium exchange pulse-labelling reveals allosteric effects in enzyme inhibition. *Lab on a Chip* **2013**, *13* (13), 2528-2532, 10.1039/C3LC00007A. DOI: 10.1039/C3LC00007A.
- (11) Seetaloo, N.; Zacharopoulou, M.; Stephens, A. D.; Kaminski Schierle, G. S.; Phillips, J. J. Millisecond Hydrogen/Deuterium-Exchange Mass Spectrometry Approach to Correlate Local Structure and Aggregation in α-Synuclein. *Anal Chem* **2022**, 94 (48), 16711-16719. DOI: 10.1021/acs.analchem.2c03183 From NLM.
- (12) Knox, R.; Lento, C.; Wilson, D. J. Mapping Conformational Dynamics to Individual Steps in the TEM-1 β-Lactamase Catalytic Mechanism. *Journal of Molecular Biology* **2018**, *430* (18, Part B), 3311-3322. DOI: https://doi.org/10.1016/j.jmb.2018.06.045.
- (13) Narang, D.; Lento, C.; J. Wilson, D. HDX-MS: An Analytical Tool to Capture Protein Motion in Action. *Biomedicines* **2020**, *8* (7), 224.

- (14) Khanal, A.; Pan, Y.; Brown, L. S.; Konermann, L. Pulsed hydrogen/deuterium exchange mass spectrometry for time-resolved membrane protein folding studies. *Journal of Mass Spectrometry* **2012**, *47* (12), 1620-1626. DOI: https://doi.org/10.1002/jms.3127.
- (15) Keppel, T. R.; Weis, D. D. Analysis of disordered proteins using a simple apparatus for millisecond quench-flow H/D exchange. *Anal Chem* **2013**, *85* (10), 5161-5168. DOI: 10.1021/ac4004979 From NLM.
- (16) Wilson, D. J.; Konermann, L. A capillary mixer with adjustable reaction chamber volume for millisecond time-resolved studies by electrospray mass spectrometry. *Anal Chem* **2003**, *75* (23), 6408-6414. DOI: 10.1021/ac0346757 From NLM.
- (17) Rob, T.; Liuni, P.; Gill, P. K.; Zhu, S.; Balachandran, N.; Berti, P. J.; Wilson, D. J. Measuring dynamics in weakly structured regions of proteins using microfluidics-enabled subsecond H/D exchange mass spectrometry. *Anal Chem* **2012**, *84* (8), 3771-3779. DOI: 10.1021/ac300365u From NLM.
- (18) Brown, K. A.; Lento, C.; Rajendran, S.; Dowd, J.; Wilson, D. J. Epitope Mapping for a Preclinical Bevacizumab (Avastin) Biosimilar on an Extended Construct of Vascular Endothelial Growth Factor A Using Millisecond Hydrogen-Deuterium Exchange Mass Spectrometry. *Biochemistry* **2020**, *59* (30), 2776-2781. DOI: 10.1021/acs.biochem.0c00308 From NLM. (19) Svejdal, R. R.; Dickinson, E. R.; Sticker, D.; Kutter, J. P.; Rand, K. D. Thiol-ene Microfluidic Chip for Performing Hydrogen/Deuterium Exchange of Proteins at Subsecond Time Scales. *Analytical Chemistry* **2019**, *91* (2), 1309-1317. DOI: 10.1021/acs.analchem.8b03050. (20) Kish, M.; Smith, V.; Lethbridge, N.; Cole, L.; Bond, N. J.; Phillips, J. J. Online Fully Automated System for Hydrogen/Deuterium-Exchange Mass Spectrometry with Millisecond Time Resolution. *Analytical Chemistry* **2023**, *95* (11), 5000-5008. DOI: 10.1021/acs.analchem.2c05310.
- (21) Song, H.; Ismagilov, R. F. Millisecond kinetics on a microfluidic chip using nanoliters of reagents. *J Am Chem Soc* **2003**, *125* (47), 14613-14619. DOI: 10.1021/ja0354566 From NLM. (22) Dressler, O. J.; Casadevall, I. S. X.; deMello, A. J. Chemical and Biological Dynamics Using Droplet-Based Microfluidics. *Annu Rev Anal Chem (Palo Alto Calif)* **2017**, *10* (1), 1-24. DOI: 10.1146/annurev-anchem-061516-045219 From NLM.
- (23) Taylor, G. I. Dispersion of soluble matter in solvent flowing slowly through a tube. *Proceedings of the Royal Society of London. Series A. Mathematical and Physical Sciences* **1953**, *219* (1137), 186-203. DOI: doi:10.1098/rspa.1953.0139.
- (24) Aris, R.; Taylor, G. I. On the dispersion of a solute in a fluid flowing through a tube. *Proceedings of the Royal Society of London. Series A. Mathematical and Physical Sciences* **1956**, *235* (1200), 67-77. DOI: doi:10.1098/rspa.1956.0065.
- (25) Song, H.; Tice, J. D.; Ismagilov, R. F. A Microfluidic System for Controlling Reaction Networks in Time. *Angewandte Chemie International Edition* **2003**, *42* (7), 768-772. DOI: https://doi.org/10.1002/anie.200390203.
- (26) Yang, T.; Buholzer, K. J.; Sottini, A.; Cao, X.; deMello, A.; Nettels, D.; Schuler, B. Rapid droplet-based mixing for single-molecule spectroscopy. *Nature Methods* **2023**, *20* (10), 1479-1482. DOI: 10.1038/s41592-023-01995-9.
- (27) Niu, X.; Gulati, S.; Edel, J. B.; deMello, A. J. Pillar-induced droplet merging in microfluidic circuits. *Lab on a Chip* **2008**, 8 (11), 1837-1841, 10.1039/B813325E. DOI: 10.1039/B813325E. (28) Stubbs, J.; Hornsey, T.; Hanrahan, N.; Esteban, L. B.; Bolton, R.; Maly, M.; Basu, S.; Orlans,
- J.; de Sanctis, D.; Shim, J.-u.; et al. Droplet microfluidics for time-resolved serial crystallography. *IUCrJ* **2024**, *11* (2), 237-248. DOI: doi:10.1107/S2052252524001799.
- (29) Martin, M. M.; Lindqvist, L. The pH dependence of fluorescein fluorescence. *Journal of Luminescence* **1975**, *10* (6), 381-390. DOI: https://doi.org/10.1016/0022-2313(75)90003-4.
- (30) Salmas, R. E.; Borysik, A. J. Deep Learning Enables Automatic Correction of Experimental HDX-MS Data with Applications in Protein Modeling. *Journal of the American Society for Mass Spectrometry* **2024**, *35* (2), 197-204. DOI: 10.1021/jasms.3c00285.

- (31) Sørensen, L.; Salbo, R. Optimized Workflow for Selecting Peptides for HDX-MS Data Analyses. *Journal of The American Society for Mass Spectrometry* **2018**, *29* (11), 2278-2281. DOI: 10.1007/s13361-018-2056-1.
- (32) Houde, D.; Berkowitz, S. A.; Engen, J. R. The Utility of Hydrogen/Deuterium Exchange Mass Spectrometry in Biopharmaceutical Comparability Studies. *Journal of Pharmaceutical Sciences* **2011**, *100* (6), 2071-2086. DOI: https://doi.org/10.1002/jps.22432.
- (33) Weis, D. D. Comment on Houde, D.; Berkowitz, S. A.; Engen, J. R., The Utility of Hydrogen/Deuterium Exchange Mass Spectrometry in Biopharmaceutical Comparability Studies. J. Pharm. Sci. 2011, 100, 2071-2086. *Journal of Pharmaceutical Sciences* **2019**, *108* (2), 807-810. DOI: https://doi.org/10.1016/j.xphs.2018.10.010.
- (34) Perez-Riverol, Y.; Bandla, C.; Kundu, D. J.; Kamatchinathan, S.; Bai, J.; Hewapathirana, S.; John, N. S.; Prakash, A.; Walzer, M.; Wang, S.; Vizcaíno, J. A. The PRIDE database at 20 years: 2025 update. *Nucleic Acids Res* **2025**, *53* (D1), D543-d553. DOI: 10.1093/nar/gkae1011 From NLM.
- (35) Fidalgo, L. M.; Abell, C.; Huck, W. T. S. Surface-induced droplet fusion in microfluidic devices. *Lab on a Chip* **2007**, *7* (8), 984-986, 10.1039/B708091C. DOI: 10.1039/B708091C. (36) Liu, Y.; Ismagilov, R. F. Dynamics of Coalescence of Plugs with a Hydrophilic Wetting Layer Induced by Flow in a Microfluidic Chemistrode. *Langmuir* **2009**, *25* (5), 2854-2859. DOI: 10.1021/la803518b.
- (37) Ahn, K.; Agresti, J.; Chong, H.; Marquez, M.; Weitz, D. A. Electrocoalescence of drops synchronized by size-dependent flow in microfluidic channels. *Applied Physics Letters* **2006**, *88* (26). DOI: 10.1063/1.2218058 (accessed 3/1/2025).
- (38) Abate, A. R.; Hung, T.; Mary, P.; Agresti, J. J.; Weitz, D. A. High-throughput injection with microfluidics using picoinjectors. *Proceedings of the National Academy of Sciences* **2010**, *107* (45), 19163-19166. DOI: doi:10.1073/pnas.1006888107.
- (39) Link, D. R.; Grasland-Mongrain, E.; Duri, A.; Sarrazin, F.; Cheng, Z.; Cristobal, G.; Marquez, M.; Weitz, D. A. Electric Control of Droplets in Microfluidic Devices. *Angewandte Chemie International Edition* **2006**, *45* (16), 2556-2560. DOI: https://doi.org/10.1002/anie.200503540.
- (40) Priest, C.; Herminghaus, S.; Seemann, R. Controlled electrocoalescence in microfluidics: Targeting a single lamella. *Applied Physics Letters* **2006**, 89 (13). DOI: 10.1063/1.2357039 (accessed 3/1/2025).
- (41) Frenz, L.; El Harrak, A.; Pauly, M.; Bégin-Colin, S.; Griffiths, A. D.; Baret, J.-C. Droplet-Based Microreactors for the Synthesis of Magnetic Iron Oxide Nanoparticles. *Angewandte Chemie International Edition* **2008**, *47* (36), 6817-6820. DOI: https://doi.org/10.1002/anie.200801360.
- (42) Mazutis, L.; Baret, J.-C.; Griffiths, A. D. A fast and efficient microfluidic system for highly selective one-to-one droplet fusion. *Lab on a Chip* **2009**, 9 (18), 2665-2672, 10.1039/B903608C. DOI: 10.1039/B903608C.
- (43) Mazutis, L.; Griffiths, A. D. Selective droplet coalescence using microfluidic systems. *Lab on a Chip* **2012**, *12* (10), 1800-1806, 10.1039/C2LC40121E. DOI: 10.1039/C2LC40121E.
- (44) Shestopalov, I.; Tice, J. D.; Ismagilov, R. F. Multi-step synthesis of nanoparticles performed on millisecond time scale in a microfluidic droplet-based system. *Lab on a Chip* **2004**, *4* (4), 316-321, 10.1039/B403378G. DOI: 10.1039/B403378G.
- (45) Li, L.; Boedicker, J. Q.; Ismagilov, R. F. Using a Multijunction Microfluidic Device To Inject Substrate into an Array of Preformed Plugs without Cross-Contamination: Comparing Theory and Experiments. *Analytical Chemistry* **2007**, *79* (7), 2756-2761. DOI: 10.1021/ac062179n.
- (46) Bremond, N.; Thiam, A. R.; Bibette, J. Decompressing Emulsion Droplets Favors Coalescence. *Physical Review Letters* **2008**, *100* (2), 024501. DOI: 10.1103/PhysRevLett.100.024501.
- (47) Hung, L.-H.; Choi, K. M.; Tseng, W.-Y.; Tan, Y.-C.; Shea, K. J.; Lee, A. P. Alternating droplet generation and controlled dynamic droplet fusion in microfluidic device for CdS nanoparticle synthesis. *Lab on a Chip* **2006**, 6 (2), 174-178, 10.1039/B513908B. DOI: 10.1039/B513908B.

- (48) Tan, Y.-C.; Fisher, J. S.; Lee, A. I.; Cristini, V.; Lee, A. P. Design of microfluidic channel geometries for the control of droplet volume, chemical concentration, and sorting. *Lab on a Chip* **2004**, *4* (4), 292-298, 10.1039/B403280M. DOI: 10.1039/B403280M.
- (49) Tam, A. C.; Patel, C. K. N. Optical absorptions of light and heavy water by laser optoacoustic spectroscopy. *Appl. Opt.* **1979**, *18* (19), 3348-3358. DOI: 10.1364/AO.18.003348. (50) Fick, A. Ueber Diffusion. *Annalen der Physik* **1855**, *170* (1), 59-86. DOI: https://doi.org/10.1002/andp.18551700105.
- (51) Agmon, N. The Grotthuss mechanism. *Chemical Physics Letters* **1995**, *244* (5), 456-462. DOI: https://doi.org/10.1016/0009-2614(95)00905-J.
- (52) Knight, C.; Voth, G. A. The Curious Case of the Hydrated Proton. *Accounts of Chemical Research* **2012**, *45* (1), 101-109. DOI: 10.1021/ar200140h.
- (53) Coales, S. J.; E, S. Y.; Lee, J. E.; Ma, A.; Morrow, J. A.; Hamuro, Y. Expansion of time window for mass spectrometric measurement of amide hydrogen/deuterium exchange reactions. *Rapid Commun Mass Spectrom* **2010**, *24* (24), 3585-3592. DOI: 10.1002/rcm.4814 From NLM.
- (54) Goswami, D.; Devarakonda, S.; Chalmers, M. J.; Pascal, B. D.; Spiegelman, B. M.; Griffin, P. R. Time Window Expansion for HDX Analysis of an Intrinsically Disordered Protein. *Journal of the American Society for Mass Spectrometry* **2013**, *24* (10), 1584-1592. DOI: 10.1007/s13361-013-0669-y.
- (55) Miyawaki, A.; Llopis, J.; Heim, R.; McCaffery, J. M.; Adams, J. A.; Ikura, M.; Tsien, R. Y. Fluorescent indicators for Ca2+based on green fluorescent proteins and calmodulin. *Nature* **1997**, *388* (6645), 882-887. DOI: 10.1038/42264.
- (56) Gilli, R.; Lafitte, D.; Lopez, C.; Kilhoffer, M. C.; Makarov, A.; Briand, C.; Haiech, J. Thermodynamic Analysis of Calcium and Magnesium Binding to Calmodulin. *Biochemistry* **1998**, *37* (16), 5450-5456. DOI: 10.1021/bi972083a.
- (57) Biekofsky, R. R.; Turjanski, A. G.; Estrin, D. A.; Feeney, J.; Pastore, A. Ab Initio Study of NMR 15N Chemical Shift Differences Induced by Ca2+ Binding to EF-Hand Proteins. *Biochemistry* **2004**, *43* (21), 6554-6564. DOI: 10.1021/bi0497852.
- (58) Park, H. Y.; Kim, S. A.; Korlach, J.; Rhoades, E.; Kwok, L. W.; Zipfel, W. R.; Waxham, M. N.; Webb, W. W.; Pollack, L. Conformational changes of calmodulin upon Ca²⁺ binding studied with a microfluidic mixer. *Proceedings of the National Academy of Sciences* **2008**, *105* (2), 542-547. DOI: doi:10.1073/pnas.0710810105.
- (59) Liu, X. R.; Rempel, D. L.; Gross, M. L. Composite Conformational Changes of Signaling Proteins upon Ligand Binding Revealed by a Single Approach: Calcium-Calmodulin Study. *Analytical Chemistry* **2019**, *91* (19), 12560-12567. DOI: 10.1021/acs.analchem.9b03491.
- (60) Babu, Y. S.; Bugg, C. E.; Cook, W. J. Structure of calmodulin refined at 2.2 Å resolution. Journal of Molecular Biology **1988**, 204 (1), 191-204. DOI: https://doi.org/10.1016/0022-2836(88)90608-0.
- (61) Chattopadhyaya, R.; Meador, W. E.; Means, A. R.; Quiocho, F. A. Calmodulin structure refined at 1.7 Å resolution. *Journal of Molecular Biology* **1992**, *228* (4), 1177-1192. DOI: https://doi.org/10.1016/0022-2836(92)90324-D.
- (62) Gifford, Jessica L.; Walsh, Michael P.; Vogel, Hans J. Structures and metal-ion-binding properties of the Ca2+-binding helix–loop–helix EF-hand motifs. *Biochemical Journal* **2007**, *405* (2), 199-221. DOI: 10.1042/bj20070255 (accessed 4/23/2025).
- (63) Ikura, M.; Clore, G. M.; Gronenborn, A. M.; Zhu, G.; Klee, C. B.; Bax, A. Solution structure of a calmodulin-target peptide complex by multidimensional NMR. *Science* **1992**, *256* (5057), 632-638. DOI: doi:10.1126/science.1585175.
- (64) Barbato, G.; Ikura, M.; Kay, L. E.; Pastor, R. W.; Bax, A. Backbone dynamics of calmodulin studied by nitrogen-15 relaxation using inverse detected two-dimensional NMR spectroscopy: the central helix is flexible. *Biochemistry* **1992**, *31* (23), 5269-5278. DOI: 10.1021/bi00138a005.

- (65) Ghosh, C.; Jana, B. Role of Calcium in Modulating the Conformational Landscape and Peptide Binding Induced Closing of Calmodulin. *The Journal of Physical Chemistry B* **2021**, *125* (9), 2317-2327. DOI: 10.1021/acs.jpcb.1c00783.
- (66) Faas, G. C.; Raghavachari, S.; Lisman, J. E.; Mody, I. Calmodulin as a direct detector of Ca2+ signals. *Nature Neuroscience* **2011**, *14* (3), 301-304. DOI: 10.1038/nn.2746.
- (67) Zhang, J.; Li, J.; Craig, T. A.; Kumar, R.; Gross, M. L. Hydrogen–Deuterium Exchange Mass Spectrometry Reveals Calcium Binding Properties and Allosteric Regulation of Downstream Regulatory Element Antagonist Modulator (DREAM). *Biochemistry* **2017**, *56* (28), 3523-3530. DOI: 10.1021/acs.biochem.7b00100.
- (68) Finn, B. E.; Evenäs, J.; Drakenberg, T.; Waltho, J. P.; Thulin, E.; Forsén, S. Calcium-induced structural changes and domain autonomy in calmodulin. *Nature Structural Biology* **1995**, *2* (9), 777-783. DOI: 10.1038/nsb0995-777.
- (69) Shukla, D.; Peck, A.; Pande, V. S. Conformational heterogeneity of the calmodulin binding interface. *Nature Communications* **2016**, *7* (1), 10910. DOI: 10.1038/ncomms10910.
- (70) Linse, S.; Helmersson, A.; Forsén, S. Calcium binding to calmodulin and its globular domains. *Journal of Biological Chemistry* **1991**, *266* (13), 8050-8054. DOI: https://doi.org/10.1016/S0021-9258(18)92938-8.
- (71) Porumb, T. Determination of Calcium-Binding Constants by Flow Dialysis. *Analytical Biochemistry* **1994**, *220* (2), 227-237. DOI: https://doi.org/10.1006/abio.1994.1332.
- (72) Black, D. J.; Selfridge, J. E.; Persechini, A. The kinetics of Ca(2+)-dependent switching in a calmodulin-IQ domain complex. *Biochemistry* **2007**, *46* (46), 13415-13424. DOI: 10.1021/bi700774s From NLM.
- (73) Meador, W. E.; Means, A. R.; Quiocho, F. A. Modulation of Calmodulin Plasticity in Molecular Recognition on the Basis of X-Ray Structures. *Science* **1993**, *262* (5140), 1718-1721. DOI: doi:10.1126/science.8259515.
- (74) Sun, B.; Kekenes-Huskey, P. M. Assessing the Role of Calmodulin's Linker Flexibility in Target Binding. *International Journal of Molecular Sciences* **2021**, *22* (9), 4990.
- (75) Kursula, P. The many structural faces of calmodulin: a multitasking molecular jackknife. *Amino Acids* **2014**, *4*6 (10), 2295-2304. DOI: 10.1007/s00726-014-1795-y.
- (76) Sun, B.; Kekenes-Huskey, P. M. Calmodulin's Interdomain Linker Is Optimized for Dynamics Signal Transmission and Calcium Binding. *Journal of Chemical Information and Modeling* **2022**, 62 (17), 4210-4221. DOI: 10.1021/acs.jcim.2c00587.